Shock Layer Radiation Measurements and Analysis for Mars Entry

Deepak Bose [1], Jay H. Grinstead[2]
NASA Ames Research Center, Moffett Field, CA 94035

David W. Bogdanoff[3]
ELORET, Inc., Moffett Field, CA 94035

and
Michael J. Wright [4]
NASA Ames Research Center, Moffett Field, CA 94035

NASA's In-Space Propulsion program is supporting the development of shock radiation transport models for aerocapture missions to Mars. A comprehensive test series in the NASA Ames Electric Arc Shock Tube facility at a representative flight condition was recently completed. The facility optical instrumentation enabled spectral measurements of shocked gas radiation from the vacuum ultraviolet to the near infrared. The instrumentation captured the nonequilibrium post-shock excitation and relaxation dynamics of dispersed spectral features. A description of the shock tube facility, optical instrumentation, and examples of the test data are presented. Comparisons of measured spectra with model predictions are also made.

I. Introduction

Radiative heating during entries in CO_2-N_2 atmospheres, such as that of Mars and Venus, will be important if the entry speed in higher than 7.5 km/s. Such entry speeds will be required for several candidate missions of interest including aerocapture maneuvers and direct entry of probes into Venus. Radiative heating will also be a significant component of heating for large entry vehicles, which would likely be the case for high mass payload landing systems on Mars. The atmosphere of Mars and Venus each consist of about 96% CO_2, 4% N_2, and a trace amount of Ar by volume. When this gas mixture is shocked, several potentially strong radiators are formed, including CO, CN, and C and O atoms. Predictions of the radiative heating generated by these species indicate that shock layer radiation will become significant at velocities above about 7.5 km/s. Radiation has not been a design concern for prior Mars missions due to a combination of low entry velocities and small entry vehicle sizes. For example, the Mars Pathfinder probe (1997) was the fastest Mars entry to date, but was predicted to encounter a maximum of only about 10 W/cm^2 of radiative heating[3] due to its small size. The much larger Mars Science Laboratory, scheduled for launch in 2009, will encounter only about 0.01 W/cm^2 of radiative heating due to its comparatively low entry velocity. Future Mars aerocapture systems, particularly those in support of crewed missions, will be larger and likely enter at higher velocities. Shock layer radiation will thus be a dominant portion of the entry heating environment for this mission class. For Venus missions, the orbital mechanics of the transfer dictate entry velocities on the order of 11 km/s. At this speed radiation will be a dominant portion of the total entry heat flux and heat load, even for small entry probes. For example, the Pioneer Venus mission consisted of four entry probes with varying destination and entry flight path angle. The peak radiative heat flux for these vehicles was predicted to range from 1300-3400 W/cm^2 (Ref. 4), or about half of the total.

To support this effort, shock layer radiation at relevant aerocapture conditions has been investigated experimentally in the NASA Ames Electric Arc Shock Tube (EAST) facility. The EAST facility has the capability to generate

[1] Aerospace Engineer, Reacting Flow Environments Branch, MS 230-3; Senior Member AIAA
[2] Senior Research Scientist, Reacting Flow Environments Branch, MS 230-2; Senior Member AIAA
[3] Senior Research Scientist, Reacting Flow Environments Branch, MS 230-2; Associate Fellow AIAA
[4] Senior Research Scientist, Reacting Flow Environments Branch, MS 230-2; Associate Fellow AIAA

shock-heated gas mixtures at velocities and pressures representative of aerocapture trajectories. The nonequilibrium gas downstream of the moving one-dimensional shock wave in the EAST is a good analogue of the gas behind the stagnation shock on the flight vehicle, missing only the flow divergence term and the boundary layer on the surface of the vehicle. Therefore, measurements of the excitation and emission processes that occur as the post-shock mixture relaxes towards equilibrium are a direct source of validation data for physics-based radiation emission and transport codes that will be applied to flight vehicle design.

The emission spectroscopy instrumentation used for EAST testing, which includes imaging and non-imaging spectrographs, enables measurements of shocked-gas radiation spectra over the entire frequency range from the vacuum ultraviolet (VUV) to the near infrared (NIR). The imaging spectrographs, in particular, can capture the non-equilibrium post-shock excitation and relaxation dynamics of dispersed spectral features from the ultraviolet (UV) to the NIR. The capabilities of the current EAST emission spectroscopy instrumentation were first demonstrated during a test program to investigate the radiation environment for a proposed aerocapture mission to Titan.[5] Data from that test series, obtained at gas compositions, free stream pressures, and shock velocities relevant to Titan aerocapture, were used to build a new finite-rate collisional-radiative model. The new model showed the previous estimates of shock layer radiance were too high by factors up to five.[6] These predictions greatly increase the attractiveness of aerocapture versus traditional chemical propulsion for future Titan missions because the heating rates and loads are now significantly reduced over previous estimates. This, in turn, reduces the mass of the vehicle's thermal protection system (TPS) and opens up the possibility of still more efficient low-density TPS materials concepts. Results from the EAST facility were also used to perform a risk assessment of the Huygens probe prior to its January 2005 entry[7] and, later, to calibrate multiple new collisional-radiative models for CN shock layer radiation prediction.[8]

The Titan test data clearly demonstrated the value of the EAST facility for shock layer radiation predictions and high-fidelity model development. The data reported here are the beginnings of a similar model development activity for Mars and Venus entries. More data are being taken now that will improve coverage of velocity, density, and wavelength space over that reported in this paper.

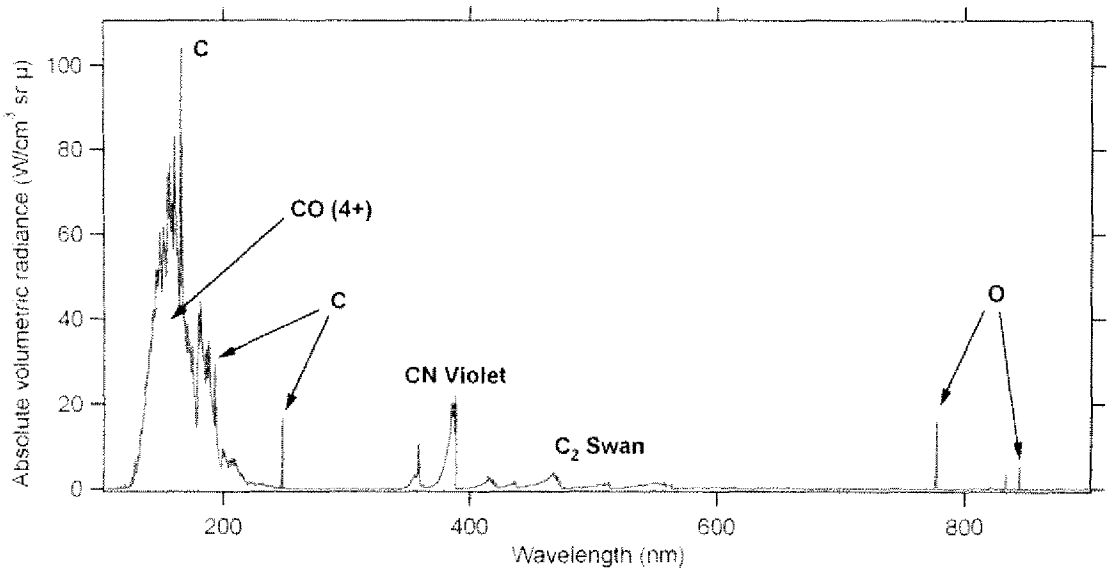

Figure 1. Predicted emission spectrum of Martian atmosphere at 8.5 km/s and 0.1 torr (13.3 Pa) pre-shock pressure

Prior researchers have used shock tubes to investigate shock layer radiation from CO_2 systems[9-13]. More recently Losev et al,[14] Zalogin et al.[15] and Kudryatsev et al.[16] conducted a series of shock tube tests in CO_2-N_2-Ar gas mixtures at velocities between 3-4 km/s and pressures from 66-660 Pa (0.5-5 Torr). These experiments were used by Zalogin et al. to develop a master equation model for CN and make estimates of the collisional excitation and de-excitation rates. These rates were later employed by Bose et al.[6] in their collisional-radiative model for Titan entries and showed good agreement with EAST data. Unfortunately, all of these shock tube test series were conducted at

low velocities and at pressures that were about an order of magnitude higher than the peak heating point on a typical Mars aerocapture vehicle. At these higher pressures nonequilibrium effects would be much smaller, making validation of a nonequilibrium radiation model appropriate for flight predictions based on these data very difficult. Also, the majority of the data from these tests measured the emission at a single wavelength as a function of time, instead of the total integrated radiative power over a large wavelength range needed to validate and calibrate computational models. Finally, these experiments focused on emission from the CN system and did not obtain quantitative data for the CO (4+) system, which is predicted to be the dominant source of shock layer radiation for Mars and Venus entries at the conditions considered in this work.

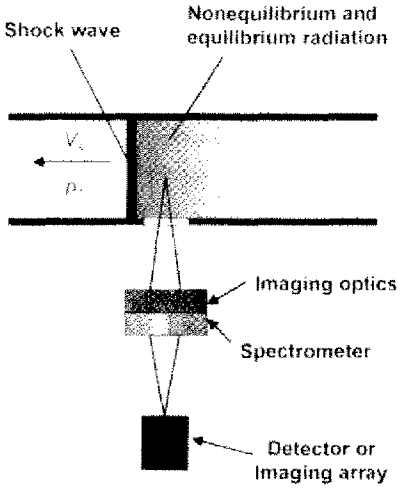

Figure 2. Emission spectroscopy instrumentation schematic.

II. Test Objectives

The test condition was chosen based on preliminary systems analyses for an aerocapture maneuver: 0.1 torr (13.3 Pa) pre-shock pressure and 8.5 km/s shock velocity. Figure 1 shows the predicted emission spectrum from the UV to the NIR, in units of absolute volumetric spectral radiance (W/cm^3 μm sr) at this condition. While the CN violet system ($B\,^2\Sigma^+ - X\,^2\Sigma^+$), C_2 Swan system ($d\,^3\Pi_g - a\,^3\Pi_u$), N_2^+ first negative system ($B\,^2\Sigma_u^+ - X\,^2\Sigma_g^+$), and several atomic carbon and oxygen lines are present, the major source of radiant energy is from the CO fourth positive system ($A\,^1\Pi - X\,^1\Sigma^+$), which radiates in the VUV portion of the spectrum (wavelengths less than ~190 nm). Measuring shock radiance in the VUV region was also of importance in the current test series.

As shock passage in a shock tube experiment is a transient event, the instrumentation used to measure shock radiance was designed have adequate spatial and temporal resolution to characterize the shock layer dynamics as the shock wave passes an observation window. The optical instrumentation is described in Section III.A. The development and validation of phenomenological models of nonequilibrium radiation require spectrally resolved measurements of absolute radiance behind a shock wave. Therefore, the spectroscopic instruments were calibrated to a reference standard spectral radiance source. Process monitoring and facility performance instrumentation was also incorporated to measure critical test parameters such as shock velocity and driven gas pressure.

III. Facility description

The EAST facility at NASA Ames Research Center was developed to simulate high-enthalpy, real gas phenomena encountered by hypersonic vehicles entering planetary atmospheres. It has the capability of producing superorbital shock speeds using an electric arc driver. The facility was built in the late 1960s to support research in aerothermochemistry of hypervelocity flight through Earth and planetary atmospheres. The use of an electric arc discharge as the driver mechanism permits generation of shock speeds up to 50 km/s in H_2/He atmospheres. These high shock speeds greatly exceed those achieved with heated light gas, combustion, or free piston drivers. A thorough description of the EAST facility can be found in Ref. 17.

A. Instrumentation

The critical instrumentation used in the experiment falls into two categories: emission spectroscopy and facility performance. The spectroscopy instrumentation was designed to measure spectrally resolved shock radiance in absolute units as the shock passes the facility windows. The shock emission is captured with collection optics that limit

the spatial volume viewed by the instrument, followed by spectral resolving instruments that disperse the emission onto single- or multi-channel high-speed photodetectors (see Fig. 2). The facility performance instrumentation, which consists of high-speed pressure transducers and transient digitizers, was used to measure shock arrival times along the driven tube. Shock velocities at the locations of the optical instruments were determined from analysis of the arrival times. Reference 18 further describes the instrumentation used in this test program.

The capability to capture more than the time-resolved emission of a single spectral feature is realized with an imaging spectrograph. In this configuration, shown schematically in Fig. 3, a monochromator is turned on its side so as to align the entrance slit in a horizontal plane, parallel to the test section axis. The collection optics image an 11 cm region, coincident with the test section axis, through a long, rectangular window in the driven tube wall. The imaged region is focused on the monochromator entrance slit. The monochromator exit slit was removed and replaced by a focal plane array, enabling a segment of the dispersed spectrum to be recorded along one axis of the array. The other axis, aligned parallel to the entrance slit, records the spatial variation of the dispersed spectrum. In this manner, spectra are recorded *simultaneously* at multiple points along the axis of the shock tube.

By using intensified CCD focal plane arrays with short exposure times, the spectral characteristics of the radiating gas behind the shock wave, and a record of how those characteristics change with distance away from the shock front, can be captured with high time resolution. The camera is triggered when the shock front nears the downstream end of the rectangular window, and the short exposure time "freezes" the shock image within the field of view of the imaging spectrograph. The shock front and the post-shock relaxation zone are recorded at one time instant with multi-point spatial resolution; i.e. the two-dimensional image captures, at a single instant, the shock radiance as a function of both wavelength and distance. This approach is analogous to a streak camera used with a non-imaging spectrograph.

Two 0.3 m monochromators were converted to imaging spectrographs. For each instrument, a spherical mirror and a flat mirror were arranged in a z-shaped configuration (see Fig. 3) to image the axis of the shock tube through a rectangular window and onto the entrance slit. Both instruments imaged the same location through identical windows on opposite sides of the shock tube. Spectrograph #1 was dedicated to measurements from approximately 190 nm to 500 nm. Spectrograph #2 was dedicated to measurements from approximately 480 nm to 900 nm. Low and high resolution gratings were used to survey wide spectral regions and capture selected atomic and molecular spectral features, respectively, as shown later in Fig. 4.

The imaging spectrographs were calibrated in wavelength using Hg, Ne, He, and deuterium spectral lamps. The spatial scale was calibrated by imaging a ruled grid placed in the object plane at the shock tube centerline. Calibration of measured signal magnitudes to absolute spectral radiance was accomplished using tungsten and deuterium radiance standard lamps. Because the radiation received by the instruments originates from a volume of gas, the radiance values are reported as W/cm^3 μm sr by normalizing the measured surface spectral radiance (W/cm^2 μm sr) to the driven tube diameter, 10.16 cm. Note that this normalization implicitly assumes that the radiant intensity of the gas is constant across the diameter (i.e. no boundary layer or curved shock effects). The spectrograph calibration procedure and sample error analyses are documented in Refs. 6 and 19.

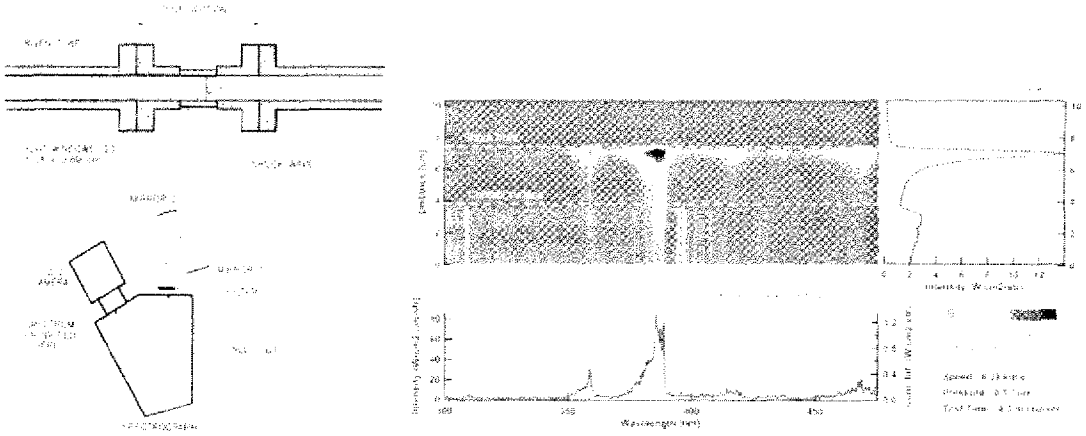

Figure 3. Schematic of one imaging spectrograph configuration (left) and example image of shock radiance at one instant in time (right) showing spectral and spatial cuts. The second imaging spectrograph simultaneously imaged the same region from the opposite side of the shock tube.

An example Spectrograph #1 image from the present experiment, calibrated in wavelength, axial distance, and absolute spectral radiance, is shown on the right of Fig. 3. The dashed lines mark the location of the shock front and contact surface. The valid test region is defined by these boundaries between the shocked driven gas and the driver gas, respectively. The arrival of the contact surface is indicated by the presence of tungsten and aluminum line radiation; these elements, along with other carbonaceous and fluorinated species, are vaporized by the arc driver and mix with the expanding driver gas. Data will be presented in the format shown in Fig. 3. The top left panel shows the absolute intensity (W/cm^2-μ-sr) as measured by the spectrograph represented using a color map over wavelength and distance in the flow direction. The top-right panel shows the integrated intensity over a wavelength range in the units of W/cm^2-sr. This panel shows the nonequilibrium overshoot and subsequent relaxation to thermochemical equilibrium characterized by steady state intensity plateau. In the ultraviolet portions of the spectrum, arrival of the driver gas in the form of metal vapor lines can often be seen. The arrival of the driver gas represents the end of useful test time. The bottom panel shows the spectra extracted by averaging intensities over a finite length behind the shock. The averaging length is chosen to represent the steady state equilibrium region downstream of the shock. The use of two imaging spectrographs covering different spectral regions, at the same spatial location, enables analysis of the simultaneous excitation and relaxation dynamics of multiple species and states.

To record emission spectra in the VUV, the optical path from the facility window through the spectrograph must be evacuated to prevent light absorption by O_2. For this test series, a vacuum-compatible monochromator was converted to a non-imaging spectrograph. A 38 mm-diameter, 500 mm-long tube couples a circular window port to the monochromator entrance slit assembly, allowing the entire optical path and the instrument to be kept under vacuum, $< 10^{-5}$ torr. Unlike for the imaging spectrographs, there are no imaging optics to convey light from the shock tube to the VUV spectrograph. The entrance slit is aligned perpendicular to the tests section axis. Circular apertures are placed inside the coupling tube to restrict the spatial resolution in the axial direction of the shock tube to approximately 1.3 mm. As with the imaging spectrographs, the monochromator exit slit assembly was removed and replaced by a focal plane array with sensitivity down to 120 nm. Available window materials, however, limited transmission to wavelengths above ~160 nm. The VUV spectrograph provides the same information as the imaging spectrographs — volumetric radiance as a function of wavelength — except there is no multi-point spatial resolution along the shock tube axis. The recorded emission originates from a spatially integrated volume, approximately 1.3 mm dia. across the 10.16 cm tube. The focal plane array was triggered at the appropriate time to capture the nonequilibrium peak of the shock radiation. As with the imaging spectrographs, signal magnitudes from the VUV spectrograph were calibrated to absolute spectral radiance units using, in this case, a deuterium reference standard lamp.

Table 1. Spectrograph instrument configurations.

Configuration	Spectrograph	Grating Density (g/mm)	Center Wavelength (nm)	Wavelength Span (nm)	Spectral resolution (nm)	Exposure time range (μs)	Features Targeted
1	1	246	268	184	0.8	0.25	CO (4+) band system; C lines
2	1	246	386	184	0.8	0.25	CNV, N_2^+ (1–) band systems
3	1	2400	358	15	0.08	0.5	CNV $\Delta v = 1$ band
4	2	150	590	227	1.7	0.25–0.5	C_2 Swan band system
5	2	150	771	227	1.7	0.25–0.5	O lines
6	2	1800	558	14	0.1	0.25–0.5	C_2 Swan $\Delta v = -1$
VUV	VUV	150	242	204	1.3	0.5	CO (4+) band system; C lines

B. Spectrograph instrument configurations and targeted spectral features

The two imaging spectrographs were configured to capture different features of the shock-heated CO_2/N_2 emission at low and high spectral resolution. The center wavelength and span determine the spectral region and extent, respectively, that were recorded for a particular configuration. Table 1 lists the gratings, spectral ranges, camera exposure times, and targeted spectral features for the 6 configurations used in the test series. The survey, or low resolution, configurations (1, 2, 4, and 5) overlap each other to ensure continuous coverage from approximately 190

nm to 880 nm with successive shots at the same nominal test condition. The exposure, or signal integration, time selected for a particular instrument configuration and test condition represents a compromise between signal-to-noise ratio and time resolution of the measurement; longer exposure times improve the signal-to-noise ratio by collecting more photons but result in spatial smearing of the image due to transit of the gas during the exposure. The amount of smearing can be estimated by considering that a shock wave moving at 8.5 km/s travels 8.5 mm in 1 μs. Higher instrument sensitivities allow for shorter exposure times to reach an acceptable signal-to-noise ratio. The center wavelength, span, and exposure time of the non-imaging VUV spectrograph configuration is also listed in Table 1. Figure 4 shows the spectral coverage of different spectrographs in each shot.

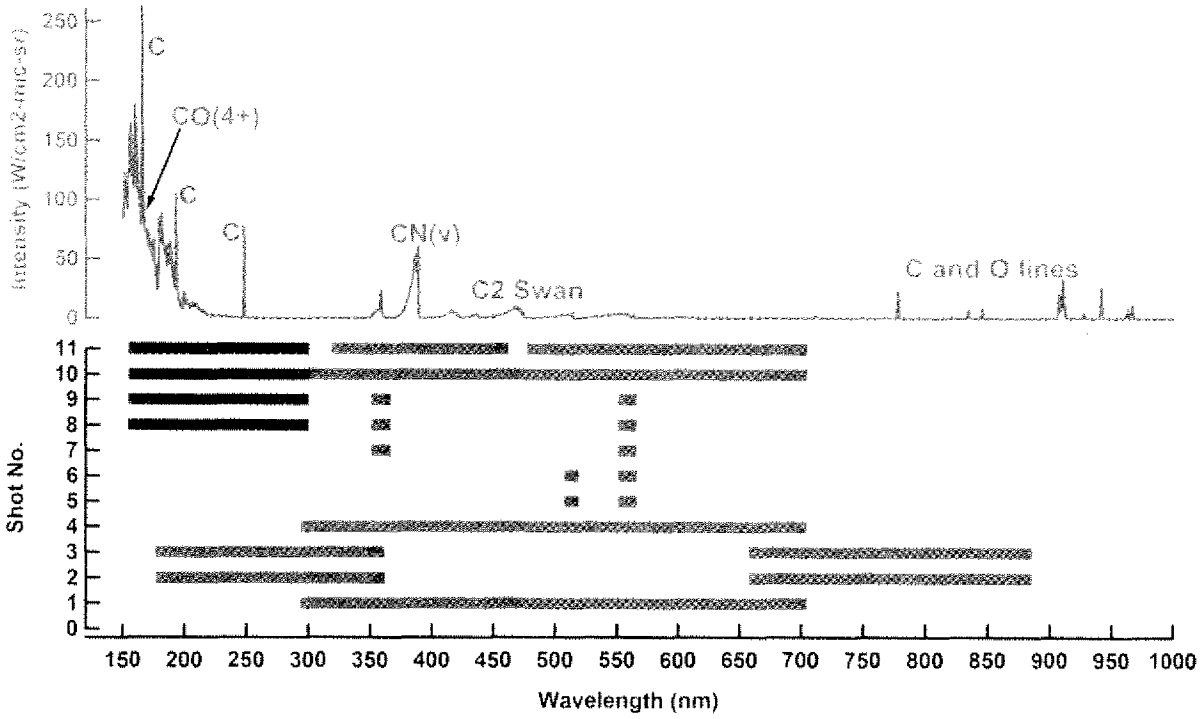

Figure 4. Predicted radiation spectrum and spectral coverage in different EAST shots. The color of the bars represent three different spectrographs described in the text.

IV. Test results and Analysis

The test gas was synthesized to a prescribed composition of 96% CO_2 and 4% N_2 by volume. The pre-shock pressure was 0.1 torr (13.3 Pa), and the target shock velocity was 8.5 km/s. As noted earlier, these conditions were chosen as representative of the peak radiative heating point on an aerocapture trajectory with an entry velocity of approximately 9 km/s, which is at the high end of trajectories considered for high mass Mars aerocapture missions. Facility variability caused an approximate ± 8% deviation from the target shock velocity over the course of the test series; however, the uncertainty in the shock velocity as measured for each run was less than ± 1%.

In this section, we will present selected data and compare them with model predictions. The modeling of shock layer radiation at NASA Ames Research Center is done using a line-by-line radiation program known as Nonequilibrium Air Radiation (NEQAIR) code.[1] NEQAIR computes spontaneous emission, absorption, and stimulated emission due to transitions between various energy states of chemical species present along a line-of-sight. Individual electronic transitions are considered for atoms and molecules. The molecular band systems are resolved for each rotational line. The molecular systems included are, CN violet and red, CO fourth positive, C_2 Swan, and several molecular bands of oxygen and nitrogen. The atomic lines of C, N, and O are included. Bound-free and free-free radiation are also considered as outlined in Ref. 1. The distribution of electronic state population is determined by a

Boltzmann distribution since a nonequilibrium master equation based model is not available for radiators in a CO_2-N_2 mixture.

As a first step in this work, since we only analyze thermochemical equilibrium radiation. The simulated spectra from the shock tube are generated using a line of sight that runs perpendicular to the tube axis assuming a constant property gas with a length equal to the diameter of the tube (see Fig. 3). The line-of-sight is chosen at a location downstream of the shock where intensity profiles have reached a steady state plateau, representing a thermochemical equilibrium state. The constant properties of the thermochemical equilibrium shocked gas are obtained from CEA.[10] The effect of the boundary layer on the tube wall is ignored.

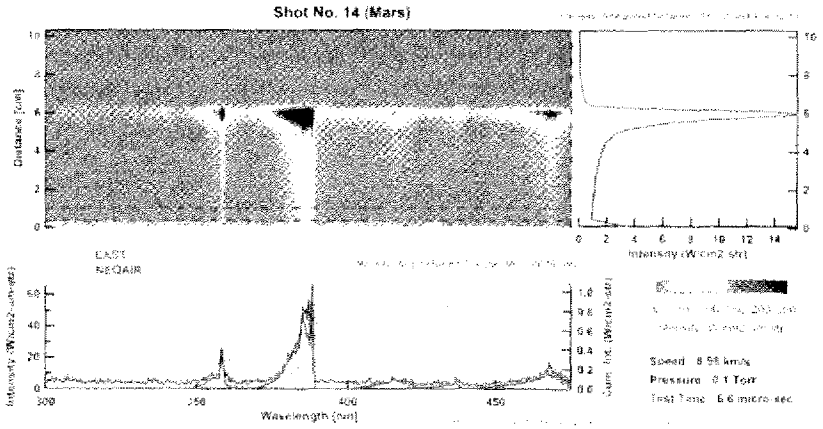

Figure 5: Comparison of NEQAIR predictions and EAST measurements in 300-475 nm range at 8.308 km/s and 0.1 Torr.

Figure 5 shows the comparison between prediction and measurement from 300-475 nm wavelength rage. Outside of the VUV, this region contains most radiation, due to CN violet and some C_2 swan bands. If the integrated area under these features is considered as a comparison metric, it is observed that CN violet radiation is slightly overpredicted by NEQAIR. This finding is not very surprising since it is known that CN(B) state is very likely underpopulated, due to radiative quenching, relative to a Boltzmann distribution. The overall integrated intensity, however, is underpredicted due to what appears to be background radiation that is seen in measurements. The background radiation of this magnitude is not predicted by NEQAIR, despite the inclusion of bound-free and free-free radiation. A similar presence of background radiation is also seen high speed air radiation shots.RRR

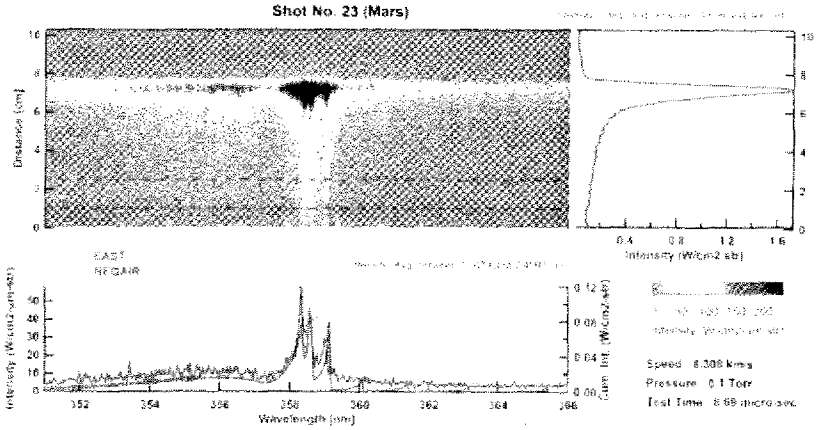

Figure 6: Comparison of NEQAIR predictions and EAST measurements in 351-356 nm range at 8.308 km/s, 0.1 Torr.

Figure 6 shows that primary manifold ($\Delta v=0$) of the CN violet radiation. The qualitative features are predicted fairly well. The overall integrated intensity is underpredicted by NEQAIR, and is, again, due to the presence of high level of background radiation.

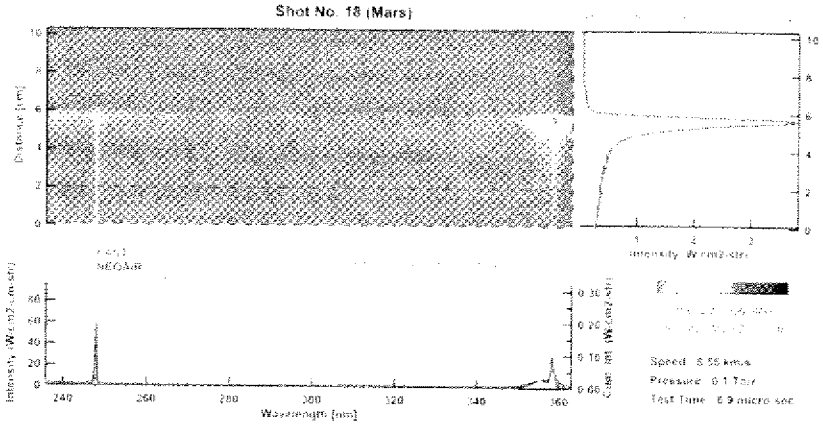

Figure 7: Comparison of NEQAIR predictions and EAST measurements in 236-363 nm range at 8.55 km/s, 0.1 Torr.

Figure 7 shows a UV region with an atomic C line at 248 nm and the CN violet ($\Delta v=+1$) manifold. The areas under both of these features are predicted fairly well. However, as seen before, the considerable background intensity measured, ultimately leads to a large underprediction of integrated intensity over this spectral spectral range. A set of tests to confirm the origin of the background radiation and to determine if it is real is underway.

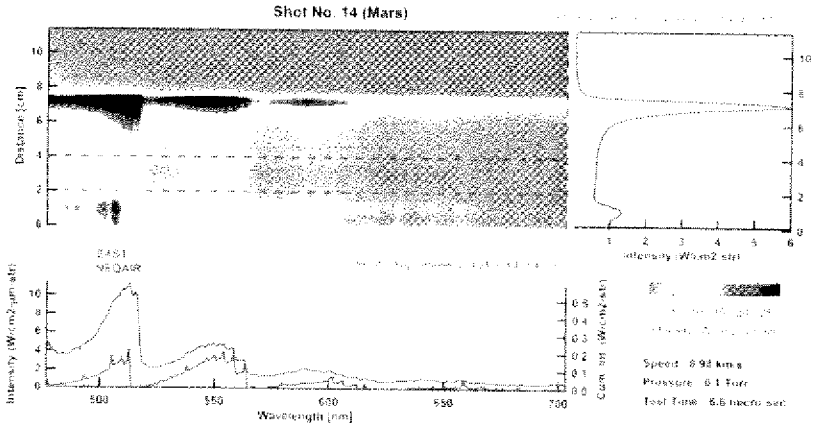

Figure 8: Comparison of NEQAIR predictions and EAST measurements in 477-703 nm range at 8.98 km/s and 0.1 Torr

Figure 8 shows different manifolds of C_2 Swan bands. The C_2 Swan intensity is generally underpredicted. It is worth noting that CN red system although weak also appears in this spectral range. The mismatch in the relative magnitude of $\Delta v=0$ and $\Delta v=-1$ intensities in the predictions may point to an opportunity to better calibrate the Frank-Condon factors.

Figure 9 shows a high resolution spectral measurement of the $\Delta v=-1$ sub-manifolds (v'-v'': 0-1,1-2,2-3) of C_2 Swan system. Although, intensities are generally underpredicted, the relative areas under these sub-manifolds can provide a wealth of information on vibrational and rotation temperatures, as well as the adequacy of Frank-Condon factors. The overall integrated intensity is underpredicted, but could be explained by the presence of background continuum radiation.

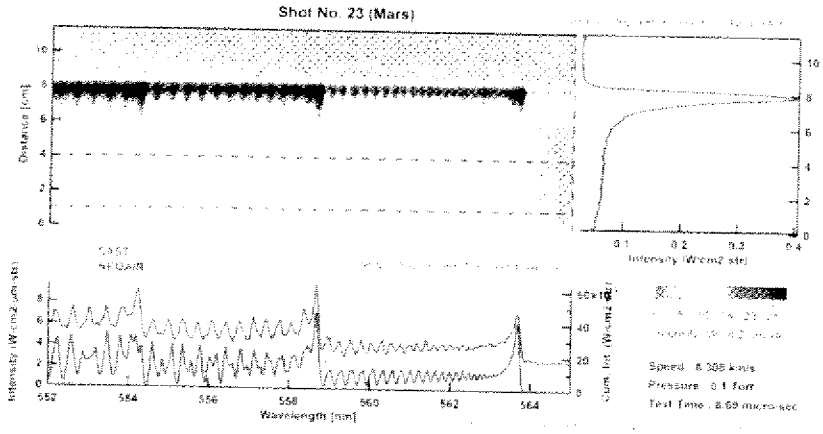

Figure 9: Comparison of NEQAIR predictions and high resolution EAST measurements in 552-565 nm range at 8.308 km/s and 0.1 Torr

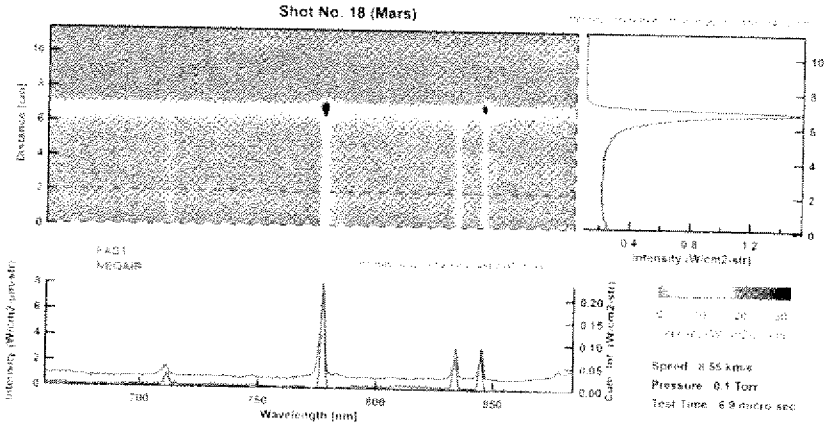

Figure 10: Comparison of NEQAIR predictions and EAST measurements in 660-884 nm range at 8.55 km/s and 0.1 Torr

Figure 10 shows the atomic lines of C and O. The overall line intensities are predicted well and can be utilized to calibrate dissociation chemistry models if applied in the nonequilibrium region. The integrated intensity, again, is underpredicted due to background continuum radiation seen in measurements.

Finally, Fig. 11 shows a sample VUV spectrum with as evacuated optical path as discussed earlier. Despite best efforts, there was evidence of air leaks into the optical path leading to measurements that are only useful in a qualitative sense. In addition, there is no spatial resolution available in the VUV spectrograph. A qualitative comparison in Fig. 10 is shown by amplifying the predicted intensity by a factor of 30 to show the spectra on a common scale with the measured spectrum. The existence of CO(4+) and C lines are observed. Future test upgrades with several instrumentation improvements will allow quantitative measurements free of ambient oxygen absorption, and will provide spatial resolution.

V. Conclusion

Shock radiation testing in the NASA Ames Electric Arc Shock Tube (EAST) facility was described. The facility has the capability to produce shocked gas conditions for the study of nonequilibrium radiation phenomena encountered by planetary atmospheric entry probes. This test program was designed to address uncertainties in radiation

transport models for used in Mars aerocapture mission studies. The instrumentation of the EAST facility enabled emission spectroscopy measurements with the spectral and spatial resolution required for analysis of the nonequilibrium shock layer excitation and relaxation kinetics. Selected results from the test series were presented and compared with predictions from NEQAIR. The preliminary analysis makes a few key observations. The molecular band radiation of CN violet is predicted well, and so are the atomic lines of C and O. C_2 Swan intensity was underpredicted. A stronger than predicted background continuum radiation with significant integrated intensity was measured. Our future tests will be targeted to resolve this discrepancy.

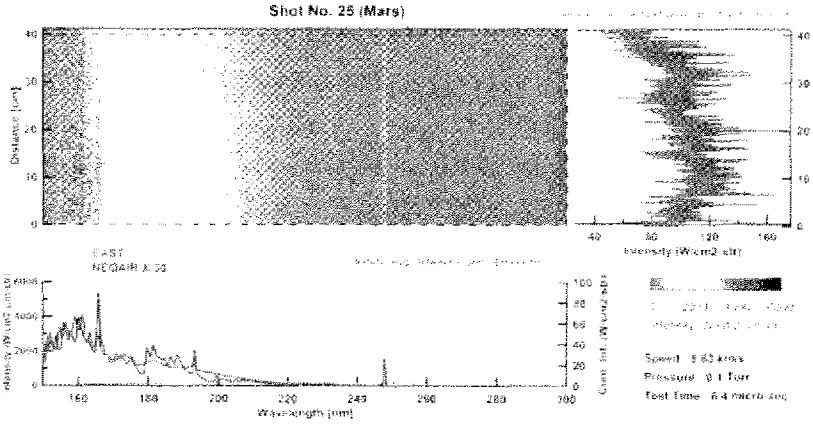

Figure 11: Sample comparison of NEQAIR predictions and the VUV-UV EAST measurements in 150-300 nm range 8.63 km/s and 0.1 Torr

Acknowledgments

This work was funded by the In-Space Propulsion program under task agreement M-ISP-03-18 to NASA Ames Research Center. The work of D. Bogdanoff and G. Allen was supported by NASA Contract NNA4BC25C to ELORET, Inc. The authors thank M. Munk and T. Kremic of NASA for their continued support of this work.

References

[1]Vaughn, D., Miller, H.C., Griffin, B., James, B.F., and Munk, M.M., "A Comparative Study of Aerocapture Missions with a Mars Destination," AIAA Paper No. 2005-4110, Jul. 2005.

[2]Lockwood, M.K. et al. "Systems Analysis for a Venus Aerocapture Mission," NASA TM 2006-214291, Mar. 2006.

[3]Milos, F.S. and Chen, Y.-K., "Mars Pathfinder Entry Temperature Data, Aerothermal Heating, and Heatshield Material Response, Journal of Spacecraft and Rockets, Vol. 36, No. 3, May 1999.

[4]Anon., "Pioneer Venus Large and Small Probe Databook," Bendix, NAS2-830Q, Jun. 1976.

[5]Lockwood, M.K., "Titan Aerocapture System Analysis," AIAA Paper No. 2003-2799, Jul. 2003.

[6]Bose, D., Wright, M., Bogdanoff, D., Raiche, G.A., and Allen, G.A., "Modeling and Experimental Assessment of CN Radiation Behind a Strong Shock Wave", *Journal of Thermophysics and Heat Transfer*, Vol. 20, 220-230, 2006.

[7]Hollis, B.R., Striepe, S.A., Wright, M.J., Bose, D., Sutton, K., and Takashima, N., "Prediction of the Aerothermodynamic Environment of the Huygens Probe," AIAA Paper No. 2005-4816, Jun. 2005.

[8]Wright, M.J., Olejniczak, J., Walpot, L., Raynaud, E., Magin, T., Caillaut, L., and Hollis, B.R., "A Code Calibration Study for Huygens Entry Aeroheating," AIAA Paper No. 2006-0382, Jan. 2006.

[9]Arnold, J.O., Reis, V.H., and Woodward, H.T., "Theoretical and Experimental Studies of Equilibrium and Nonequilibrium Radiation to Bodies Entering Postulated Martian and Venusian Atmospheres at High Speeds," AIAA Paper No. 65-0166, Jan. 1965.

[10]Thomas, G.M., and Menard, W.A., "Experimental Measurements of Nonequilibrium and Equilibrium Radiation from Planetary Atmospheres," *AIAA Journal*, Vol. 4, No. 2, 1966, pp. 227-237.

[11]Nealy, J.E., and Haggard, K.V., "A Shock Tube Study of Radiation Behind Shock Waves in CO_2 with Application to Venus Entry," *Recent Developments in Shock Tube Research: Proceedings of the 9th International Symposium on Shock Tubes and Waves*, edited by D. Bershader and W. Griffith, Stanford Univ. Press, Stanford, CA, 1973, pp. 330-339.

[12]Nealy, J.E., "An Experimental Study of Ultraviolet Radiation Behind Incident Normal Shock Waves in CO_2 at Venusian Entry Speeds," AIAA No. Paper 75-1150, Sept. 1975.

[13]Arnold, J.O., and Nicholls, R.W., "A Shock-Tube Determination of the CN Ground State Dissociation Energy and Electronic Transition Moments for the CN Violet and Red Band Systems," *Recent Developments in Shock Tube Research: Proceedings of the 9th International Symposium on Shock Tubes and Waves*, edited by D. Bershader and W. Griffith, Stanford Univ. Press, Stanford, CA, 1973, pp. 340-351.

[14]Losev, S.A., et al., "Radiation of a Mixture CO_2–N_2–Ar in Shock Waves: Experiment and Modeling," *Proceedings of the 3rd European Symposium on Aerothermodynamics for Space Vehicles*, 1998.

[15]Zalogin, G., Kozlov, P., Kuznetsova, L., Losev, S., Makarov, V., Romanenko, Y., and Surzhikov, S., "Radiation Excited by Shock Waves in a CO_2–N_2–Ar Mixture: Experiment and Theory," *Technical Physics*, Vol. 71, No. 6, 2001, pp. 10-16.

[16]Kudryatsev, N.N., Kuznetsova, L.A. and Surzhikov, S.T., "Kinetics and Nonequilibrium Radiation of CO_2–N_2 Waves," AIAA Paper No. 2001-0272, Jan. 2001.

[17]Sharma, S.P., and Park, C., "Operating Characteristics of a 60-cm and 10-cm Electric Arc Driven Shock Tube, Part I: The Driver; Part II: The Driven Section", *Journal of Thermophysics and Heat Transfer*, Vol. 4, 259-265; 266-272, 1990.

[18]Grinstead, J.H., Wilder, M.C., Olejniczak, J., Bogdanoff, D.W, Allen, G.A., Dang, K., and Forrest, M.J., "Shock-heated Air Radiation Measurements at Lunar Return Conditions", AIAA Paper No. 2008-1244, Jan. 2008.

[19]Grinstead, J.H., Olejniczak, J., Wilder, M.C., Bogdanoff, M.W., Allen, G.A, and Lillard, R., "Shock Heated Air at Lunar Return Conditions: Phase I EAST Test Report", NASA EG-CAP-07-142, 2007.

[20]Whiting, E.E., Yen, L., Arnold, J.O., and Paterson, J.A., "NEQAIR96, Nonequilibrium and Equilibrium Radiative Transport and Spectra Program: User's Manual," NASA RP-1389, Dec. 1996.

[21]Gordon, S. and McBride, B.J., "Computer Program for Calculation of Complex Chemical Equilibrium Compositions and Applications," *NASA RP 1311, Oct. 1994.*

[22]Bose, D., McCorkle, E, Thompson, C., Bogdanoff, D., Prabhu, D., Allen, G., and Grinstead, J., "Analysis and Model Validation of Shock Layer Radiation in Air," *AIAA-2008-1246, Presented at the 46th AIAA Aerospace Sciences Meeting, Reno, NV, Jan 2008.*

[23]Bose, D., McCorkle, E, Bogdanoff, D., and Allen, G., "Comparisons of Air Radiation Models with Shock Tube Measurements," *AIAA-2009-1030, Presented at the 47th AIAA Aerospace Sciences Meeting, Orlando, FL Jan 2009.*